Simultaneous Measurements of Turbulent Velocity and Sediment Motion under Tidal Bores

Nazanin Khezri
Ph.D. student, The University of Queensland, School of Civil Engineering, Brisbane QLD4072, Australia.

Hubert Chanson
Professor, The University of Queensland, School of Civil Engineering, Brisbane QLD4072, Australia.
E-mail: h.chanson@uq.edu.au

ABSTRACT: A tidal bore is a series of waves propagating upstream in a river mouth as the tide starts rising. The transient sediment motion beneath a breaking bore was investigated by measuring simultaneously the fluid and sediment motion in laboratory. Although there was no sediment transport observed during the initially steady flow, a transient sediment sheet flow motion was observed beneath the breaking bore. The sediment transport was initiated during the passage of the roller toe, when the discontinuity of the free-surface slope induced a large longitudinal pressure gradient force. The particles were subjected to large horizontal accelerations, with between 5 and 10% of all particles being subjected to maximum accelerations larger than 1 g. The particles were advected upstream with an average velocity close to the instantaneous fluid velocity. The present data provided some quantitative data in terms of various force terms acting on sediment particles beneath a tidal bore.

KEY WORDS: Tidal bores, Bed load, Transient sheet flow, Turbulence, Physical modelling.

1 INTRODUCTION

A tidal bore is a series of waves propagating upstream in a estuary as the tide starts to rise (Peregrine 1966). The existence of the bore is associated with a large tidal amplitude amplified by the estuarine channel bathymetry and relatively low freshwater discharge to satisfy basic momentum considerations (Lighthill 1978). The tidal bore is a discontinuity in terms of water depth and velocity field at the bore front (Tricker 1965). Figure 1 shows a breaking tidal bore in a laboratory channel. The shape of the bore is closely associated with its Froude number Fr defined as: $Fr = (V_o+U)/(g\times A_o/B_o)^{1/2}$ where V_o is the initial flow velocity positive downstream, U is the bore celerity positive upstream, g is the gravity acceleration, and A_o and B_o are respectively the initial flow cross-section area and free-surface width. For $1 < Fr < 1.3$ to 1.6, the bore is undular: the leading edge is a smooth wave followed by a train of free-surface undulations (Treske 1994, Koch and Chanson 2008). For larger Froude numbers, a breaking tidal bore is observed with a marked roller extending across the whole channel width (Fig. 1). The flow properties immediately in front of and behind the bore are linked to by the continuity and momentum principles (Liggett 1994, Chanson 2012).

Some field observations highlighted the bed erosion and sediment convection induced by bores (Chen et al. 1990, Chanson et al. 2011). A series of laboratory experiments were conducted recently with fixed and mobile bed (Khezri and Chanson 2012a,b). The velocity measurements during the tidal bore propagation showed that both normal Reynolds stresses and turbulent kinetic energy (TKE) were on average 10 to 30% higher on the mobile bed than on the fixed bed, at the same relative bed elevation for the same Froude number, throughout the entire water column (Fig. 2). An intense transient sheet flow motion of sliding and rolling particles was observed beneath the breaking roller. The force estimates showed that the longitudinal pressure gradient force was the dominant contribution de-stabilising the

particles and inducing the onset of sediment motion (Khezri and Chanson 2012b). Within some approximation, the drag force added a sizeable contribution to maintain the upstream particle motion, although the entire sheet flow motion was brief.

Herein the instantaneous forces acting on the sediment particles were calculated based upon simultaneous measurements of fluid velocity and particle motion. This was not conducted to date. The aim of this study is to ascertain the relative impact of instantaneous forces acting on a gravel bed during a tidal bore. After a presentation of the methodology, the basic results are detailed and discussed.

2 STUDY METHOD

2.1 Theoretical considerations

When a bore propagates over a movable bed, the forces acting on each non-cohesive sediment particle encompass the gravity force, the buoyancy force, the drag force, the lift force, the intergranular force resultant, the longitudinal pressure gradient, the virtual mass force, the Magnus force, and the Basset history force (Fig. 3A). For a single particle on a horizontal channel bed, Newton's law of motion applied to the sediment particle in the longitudinal flow direction gives in first approximation:

$$m_s \times \frac{\partial V_s}{\partial t} = F_{drag} + F_p + F_{virtual} + (F_{grain})_x + F_{Magnus} + F_{Basset} \quad (1)$$

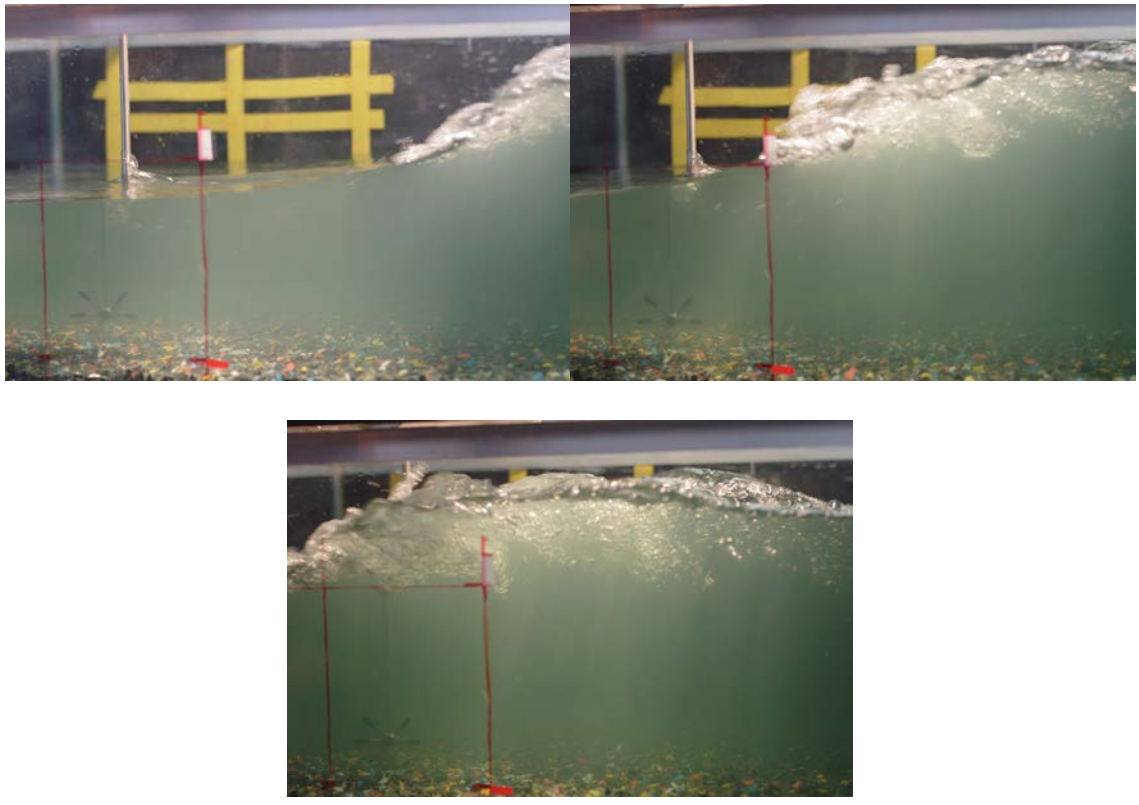

Figure 1 Sediment motion beneath a breaking tidal bore - Flow conditions: $S_o = 0$, $Q = 0.050$ m^3/s, $d_o = 0.141$ m, Fr = 1.4, mobile gravel bed - Bore motion from right to left - Sequence of three photographs (5.2 fps) with 0.19 s in between - Note the ADV unit located at x = 5 m on the left of the photographs

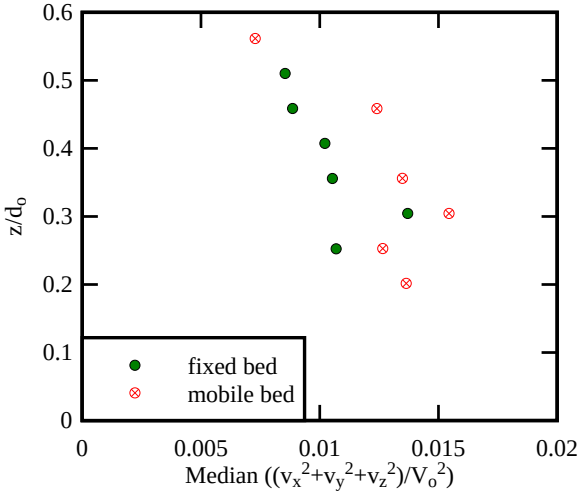

Figure 2 Vertical distributions of turbulent kinetic energy beneath a breaking tidal bore (Data: Khezri and Chanson 2012a) - Flow conditions: Q = 0.05 m^3/s, d_o = 0.14 m, Fr = 1.4, S_o = 0.002, fixed and mobile gravel beds

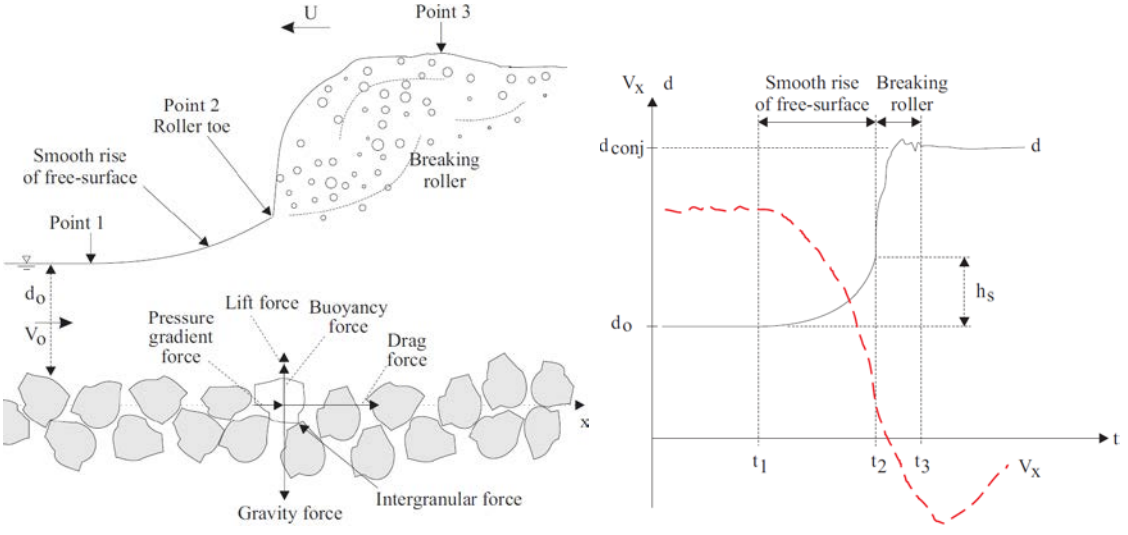

Figure 3 Propagation of a breaking bore above a movable gravel bed: (A, Left) definition sketch; (B, Right) time-variations of water elevation and longitudinal velocity

where m_s is the individual particle mass, V_s is the horizontal particle velocity component positive downstream. In Equation (1), the forces acting on a particle initially at rest are the drag force F_{drag}, a longitudinal pressure gradient force F_p, a virtual mass force $F_{virtual}$, the intergranular force component in the horizontal direction $(F_{grain})_x$ and the Basset history force F_{Basset}. When the particle is initially at rest, the Basset history force term is small, and the intergranular force resultant is commonly unknown. Each other instantaneous force term may be calculated as a function of the sediment and fluid flow properties:

$$m_s \times \frac{\partial V_s}{\partial t} = \frac{1}{2} \times C_d \times \rho \times (V_x - V_s) \times |V_x - V_s| \times A_s - \frac{\partial P}{\partial x} \times \frac{\pi \times {d_s}^3}{6} + \frac{m_s}{s} \times C_m \times \frac{\partial (V - V_s)}{\partial t} \quad (2)$$

where C_d is the drag coefficient, ρ is the water density, V_x is the longitudinal fluid velocity component positive downstream, $|V_x|$ is the velocity component magnitude, A_s is the projected area of particle, $\partial P/\partial x$ is the longitudinal pressure gradient beneath a tidal bore, x is the longitudinal direction positive downstream, d_s is the particle diameter, s is the particle relative density and C_m is an added mass

coefficient (Khezri and Chanson 2012b).

Herein the net total force and each force term listed in Equation (2) were calculated based upon the simultaneous measurements of instantaneous fluid and sediment velocities. This approach differs from the earlier study of Khezri and Chanson (2012b) who measured separately the fluid and sediment velocities, thus inferring the force estimates based upon a mean fluid velocity trend, as sketched in Figure 3B.

2.2 Laboratory investigations

New laboratory experiments were conducted in a 12 m long 0.5 m wide flume (Fig. 1). The channel invert was horizontal. The bed consisted of a series of plywood sheets covered by natural blue granite gravels (s=2.65) sieved between 4.75 mm and 6.70 mm, glued in resin and covered by a spray gloss surface finish. About x = 5 m, a 1 m long section of smooth-painted plywood sheet was covered by a layer of loose gravels, spread evenly before each run. The mobile bed layer was made of the same gravel material. (A very similar setup was used by Khezri and Chanson (2012a,b).) A fast-closing tainter gate was installed at the channel downstream end (x = 11.15 m), where x is the distance from the channel upstream end. The water discharge was supplied by a constant head reservoir and it was measured with an orifice meter designed based upon the British Standards and calibrated on site. The steady flow depths were measured using pointer gauges. The unsteady water depths were recorded non-intrusively using a series of acoustic displacement meters Microsonic™ Mic+25/IU/TC, which were calibrated against the pointer gauges in steady flows. Note that the water depth was measured above the top of the gravel bed using a 25.1 cm^2 area semi-circular footing.

The instantaneous velocity components were measured using an acoustic Doppler velocimeter (ADV) Nortek™ Vectrino+, equipped with a side-looking head, located at x = 5 m. The velocity range was 1.0 m/s and the sampling rate was 200 Hz. The translation of the ADV probe in the vertical direction was controlled by a fine adjustment travelling mechanism connected to a Mitutoyo™ digimatic scale unit, with an error of less than 0.025 mm. For all the measurements, the ADV control volume was located on the channel centreline. The post-processing of the ADV signal was limited to a removal of communication errors, although the quality of vertical velocity component V_z data was affected by the bed proximity for z < 0.030 m. The sediment particle motion was studied using a digital HD video camera recorder Sony™ HDR-SR11E/SR12E, with a field of view covering 4.5 < x < 5.5 m. Particle tracking was performed using a frame by frame analysis, for more than 200 particles in about 40 runs. For each experimental run, the video camera and ADV were synchronised mechanically within 0.01 to 0.05 s.

The tidal bore was generated by the rapid closure of the downstream gate. The closure time was between 0.1 and 0.15 s. Such a closure time was small enough to have a negligible effect on the bore propagation. For all observations, the initial flow conditions were $Q = 0.050$ m^3/s, $d_o = 0.0140$ m and $V_o = 0.714$ m where d_o and V_o are the flow depth and depth-averaged velocity measured at x = 5 m. No sediment motion was observed in the initially steady flow. The rapid gate closure generated a tidal bore propagating upstream against the initially steady flow. The simultaneous velocity and video recordings were conducted about x = 5 m for a breaking bore, for which the bore celerity was $U \approx 0.84$ m/s, corresponding to a Froude number $(V_o+U)/(g \times d_o)^{1/2} = 1.3$ to 1.4.

3 RESULTS AND DISCUSSION

3.1 Basic results

Some visual observations were conducted with both undular and breaking bores for the same identical initial flow conditions. No sediment motion was seen during the initially steady flow motion nor during the upstream propagation of undular bores (Fr < 1.3). In the breaking tidal bores, on the other hand, a large number of particles were set into motion and moved upstream behind the bore (Fig. 1). Figure 1 presents three photographs during the breaking bore passage at x = 5 m, with 0.19 s between each photograph. The transient sediment motion was mostly a sheet flow with bed load transport as reported by Khezri and Chanson (2012b). But the visual observations highlighted a broad range of sediment motion patterns, ranging from particles with almost no motion to a few saltating gravel particles subjected to a high initial acceleration. Figures 4A and 4B show the free-surface profile of a breaking

bore and the longitudinal velocity data next to the bed at x = 5 m. Both instantaneous measurements and ensemble-averaged data are included. The onset of sediment motion was associated primarily, although not always, with the passage of the roller toe (Point 2, Fig. 3). The fluid velocity data indicated a rapid flow deceleration during the bore passage, with a transient fluid recirculation next to the bed (Figs. 3B & 4B).

The sediment particle trajectories were documented for each run. Figure 4C shows five trajectories (from start to stop) together with the location of the bore characteristic points (Points 1 to 3). Two main patterns were observed: some particles were convected rapidly (particles A & C, Fig. 4C), while others were displaced upstream at a lower speed (particles B, C & E, Fig. 4C). The properties of the sediment particle motion were recorded in terms of the maximum and mean gravel particle velocities, maximum acceleration and travel duration. The maximum accelerations of the particles during the passage of the bore were recorded and the data are presented in Figure 4D. The median maximum acceleration was about 0.5 g and about 5% of particles were subjected to a maximum horizontal acceleration greater than 1 g. The maximum accelerations were found to occur mostly immediately after the bore toe ($t-t_2 > 0$) with $t = t_2$ corresponding to the roller toe passage (Point 2) as illustrated in Figure 4C.

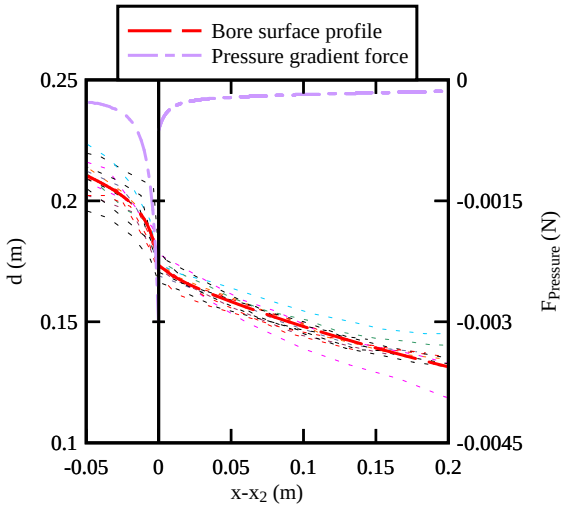

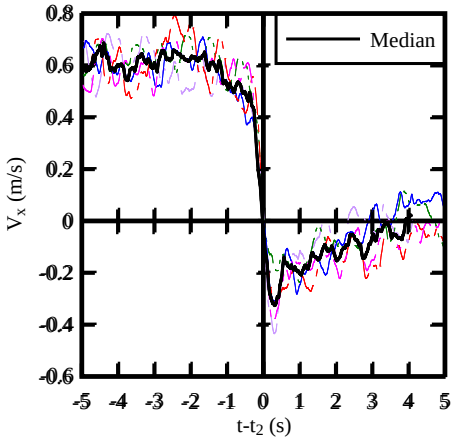

(A, Left) Instantaneous and mean free-surface profile and longitudinal pressure gradient force
(B, Right) Time-variation of the longitudinal velocity component at $z/d_o = 0.041$

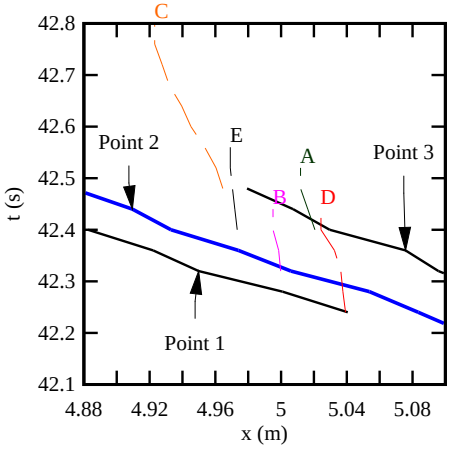

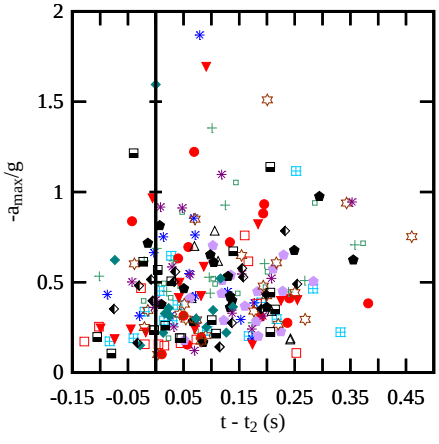

(C, Left) Sediment particle trajectories as function of time for an experimental run
(D, Right) Maximum sediment particle acceleration as a function of the relative bore passage time

Figure 4 Flow properties and sediment motion beneath a breaking tidal bore - Flow conditions: $S_o = 0$, $Q = 0.05$ m^3/s, $d_o = 0.14$ m, $V_o = 0.71$ m/s, $U = 0.84$ m/s, $Fr = 1.4$, $x = 5$ m, movable boundary bed

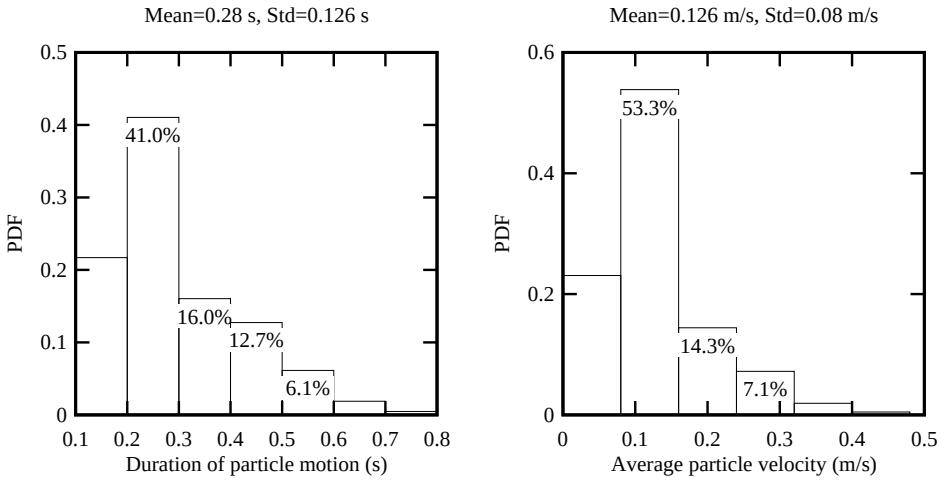

(A, Left) Particle motion duration; (B, Right) average particle velocity -$(V_s)_{mean}$

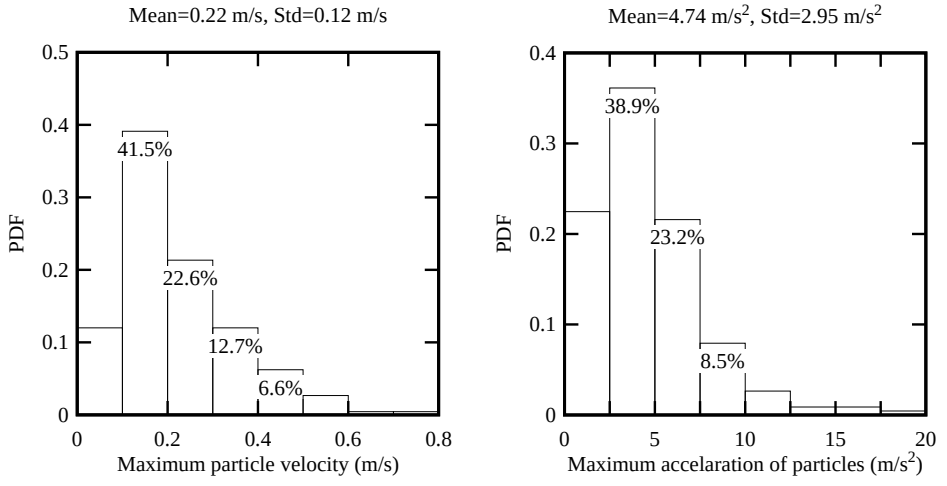

(C, Left) Maximum instantaneous particle velocity -$(V_s)_{max}$; (D, Right) Maximum particle acceleration -a_{max}

Figure 5 Sediment particle motion properties beneath a breaking tidal bore - Flow conditions: $S_o = 0$, $Q = 0.05$ m^3/s, $d_o = 0.14$ m, $V_o = 0.71$ m/s, $U = 0.84$ m/s, $Fr = 1.4$, $x = 4.5$-5.5 m movable boundary bed

The duration of sediment gravel motion was brief during the bore passage and the data are presented in Fig. 5A. About 63% of particle motion lasted less than 0.3 s. The particle average and maximum velocities during the passage of the bore are summarised in Figures 5B and 5C. The particle velocities were on average $(V_s)_{mean} \approx -0.13$ m/s (i.e. $(V_s)_{mean}/U \approx -0.15$), with the negative sign reflecting the upstream motion of the sediment particles. For comparison, the transient negative fluid velocities observed close to the bed were: $V_x/U \approx -0.25$ to -0.45 at $z/d_o = 0.08$. That is, the transient (negative) fluid and particle velocities were of comparable magnitude. The maximum particles velocities reached values up to $(V_s)_{max} \approx -0.22$ (i.e. $(V_s)_{max}/U \approx -0.26$).

3.2 Forces acting on sediment particles

The forces acting on the bed sediment particles were estimated based upon the simultaneous measurements of the free-surface properties, instantaneous velocity components next to the bed and instantaneous particle velocity. While the net force ($F = m_s \times a$) acting on each particle, where $a = \partial V_s/\partial x$ is the particle acceleration, was calculated as in Khezri and Chanson (2012b), the drag and virtual mass force terms were calculated using the instantaneous velocities, and the longitudinal pressure gradient force was deduced from the bore free-surface profile assuming hydrostatic pressure distributions. The Boussinesq equation was tested to account for the free-surface curvature, and the results showed less than

5% difference from the hydrostatic pressure estimates. The time-variation of the pressure gradient force is presented in Figures 4A and 6. In the initially steady flow, the longitudinal pressure force was zero, while the pressure gradient tended to a quasi-infinite value at the roller toe (Point 2). Figure 6 shows the instantaneous forces acting on two particles during a same run. Herein $t\text{-}t_2=0$ corresponded to the moment when the bore roller toe passed right above the particle. The fluid velocity measurements were synchronised with the video recording, the ADV head being located on the gravel bed with the sampling volume: i.e., z = 5.8 mm above the bed, compared to $d_s \approx 5.7$ mm.

The full results are summarised in Figure 7 for more than 200 particles, and a line of best fit was added for the net, drag and virtual mass force terms. A number of trends were observed. The longitudinal pressure gradient induced a dominant force term during the roller toe passage (Fig. 7). All the data indicated that the pressure gradient force was mostly responsible for the onset of bed load motion. The net force was negative during the bore passage before tending to positive values leading to the particle motion stoppage (Fig. 7A). The instantaneous virtual mass force term was non negligible (Fig. 7B). For a large majority of particles, the instantaneous drag force contributed to the upstream sediment motion during the transient flow recirculation, adding to the pressure gradient force, although for a short duration (Fig. 7C). For a very small number of particles, a relatively large positive drag force was observed, opposing the sediment particle movement (Fig. 7D).

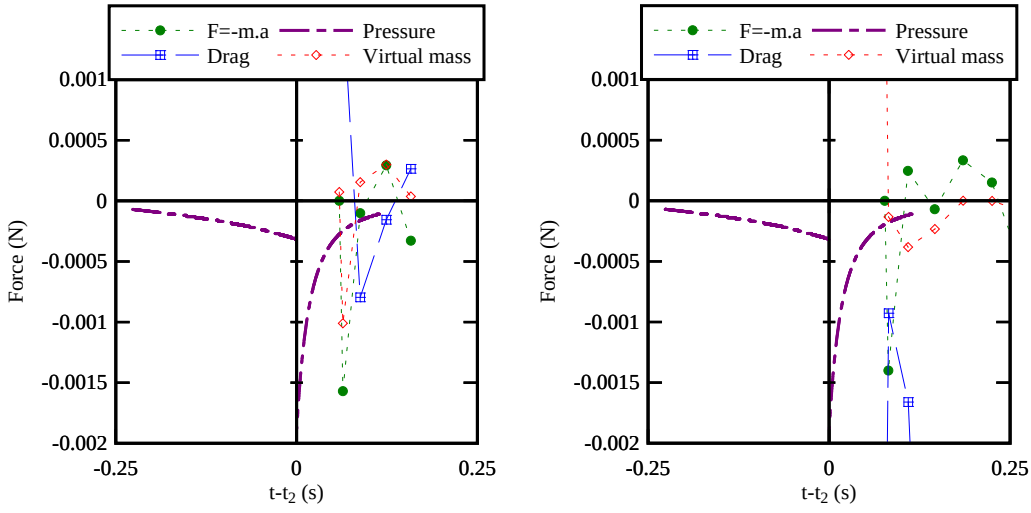

Figure 6 Instantaneous net, pressure gradient, drag and virtual mass forces acting on a sediment particle beneath a breaking tidal bore for two particles during the same experimental run - Flow conditions: $S_o = 0$, $Q = 0.05$ m^3/s, $d_o = 0.14$ m, $V_o = 0.71$ m/s, U = 0.84 m/s, Fr = 1.4, x = 4.5-5.5 m, movable boundary bed

4 DISCUSSION

The visual observations suggested that some particles were lifted up at the onset of motion before the bed load motion. The lift force on a sediment particle was estimated as:

$$F_{lift} = C_L \times \frac{\pi}{8} \times {d_s}^2 \pm \rho \times (V_x - V_s)^2 \quad (3)$$

where the lift coefficient was calculated following Mei (1982) (see also Jang et al. 2011). The results indicated that the ratio of lift to relative weight forces was about 0.24 during the steady flow conditions and decreased towards less than 0.05 during the bore roller propagation. Simply the lift force could not counterbalance the particle's submerged weight. In turn, it is believed that the apparent upward motion of some particles was likely caused by some intergrannular reaction force when the particles were dislodged.

Altogether the present data indicated that the combination of pressure gradient and drag force terms contributed primarily to the sediment sheet flow motion. The finding was validated altogether with over 400 particles, including the data set of Khezri and Chanson (2012b). The sediment movements were mostly a transient bed load motion, of relatively short duration, and the instantaneous lift force estimates

did not support the occurrence of particle saltation. The gravel particle motion was characterised by large maximum acceleration, with a median maximum acceleration of nearly 0.5 g and about 5 to 10% of particles being subjected to a maximum horizontal acceleration greater than 1 g.

At the same time, some distinctive differences were observed between the present study and that of Khezri and Chanson (2012b) based upon some average velocity estimate. In particular the present data indicated that the virtual mass force term was non negligible.

Although the particle-particle collisions were not recorded, the inter-granular force magnitude was deduced from Newton's law of motion applied to individual particles, and by testing the validity of Equation (2). The present findings suggested that the effects of inter-granular forces were possibly the most relevant at the onset of particle motion and during the particle motion stoppage.

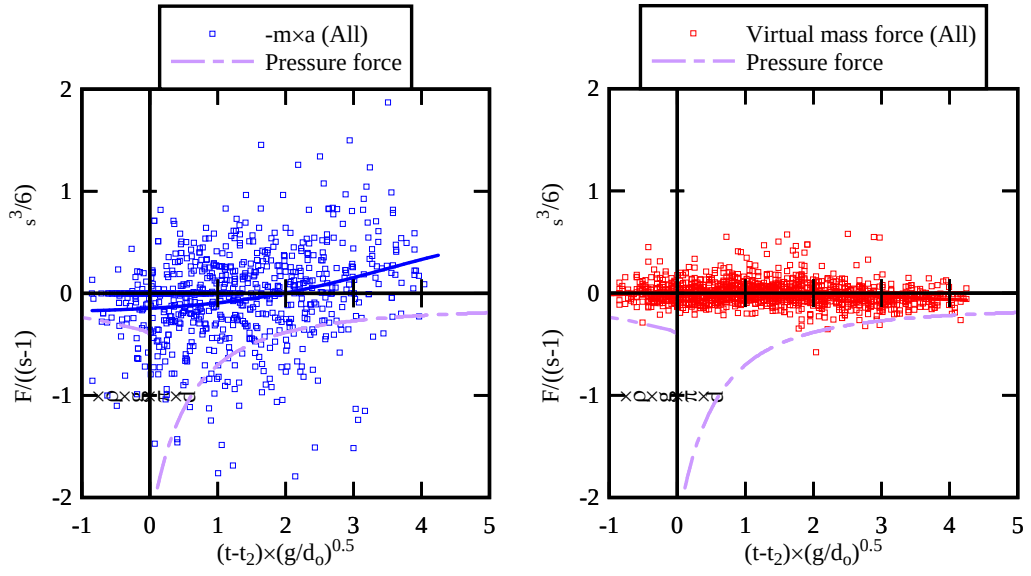

(A, Left) Net force; (B, Right) Virtual mass

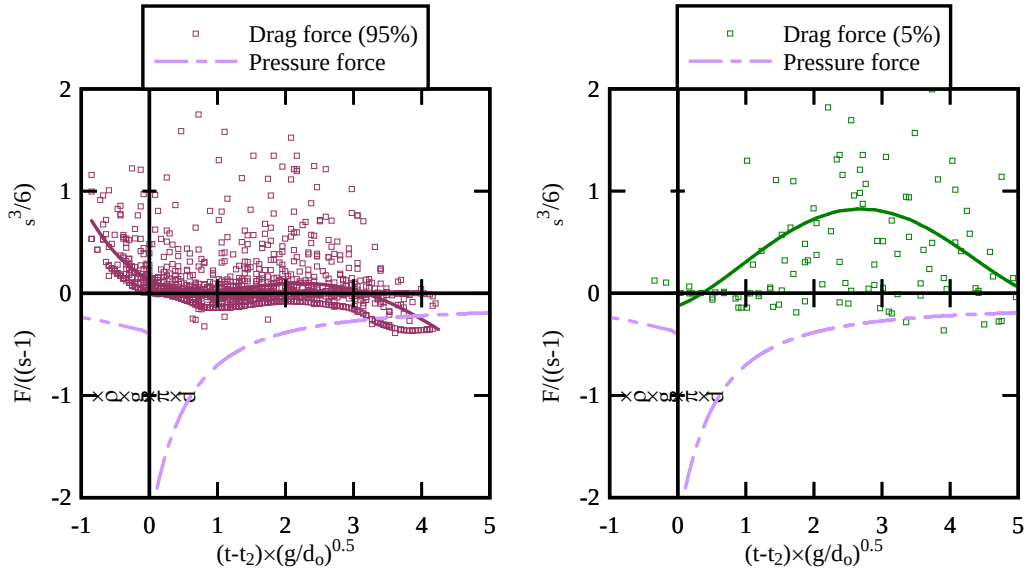

(C, Left) Drag force for 95% of particles; (D, Right) Drag force for 5% of particles

Figure 7 Instantaneous dimensionless forces acting on each sediment particle beneath a breaking tidal bore - Flow conditions: S_o = 0, Q = 0.05 m^3/s, d_o = 0.14 m, V_o = 0.71 m/s, U = 0.84 m/s, Fr = 1.4, x = 4.5-5.5 m, movable boundary bed

5 CONCLUSION

The transient sediment motion beneath a breaking bore was investigated in laboratory by measuring simultaneously the fluid and sediment motion. The study investigated a tidal bore propagating upstream against an initially steady flow with a movable bed consisting of non-cohesive gravel materials. Although there was no sediment transport observed during the initially steady flow nor beneath the undular bores, a characteristic transient sediment sheet flow motion was observed beneath the breaking bore. The data showed that the sediment transport was initiated during the passage of the roller toe (Point 2), when the discontinuity of the free-surface slope induced a large longitudinal pressure gradient force.

During the laboratory experiments, the free-surface properties, and fluid and sediment velocities, were recorded simultaneously. The particles were subjected to large horizontal accelerations, with between 5 and 10% of all particles being subjected to maximum accelerations larger than 1 g. The particles were advected upstream with an average velocity of magnitude similar to the instantaneous fluid velocity. The sediment transport was caused by the longitudinal pressure gradient force complemented by a drag force term during the transient fluid recirculation, although the entire sheet flow motion was brief.

The present study complemented the earlier study of Khezri and Chanson (2012b), demonstrating the potential for tidal bores to scour the bed sediments and to advect upstream the materials in a natural estuarine system. The findings were consistent with a number of prototype observations showing that the arrival of a tidal bore front is associated with intense bed material mixing and upstream sediment advection behind the bore front (Chen et al. 1990, Tessier and Terwindt 1994, Mouazé et al. 2010, Chanson et al. 2011, Reungoat et al. 2012). The present data provided some quantitative data in terms of various force terms acting on sediment particles beneath a tidal bore.

ACKNOWLEDGEMENTS

The authors thank Dr Pierre Lubin (University of Bordeaux) for his comments and advice. They acknowledge the technical assistance of Graham Illidge, Ahmed Ibrahim and Jason Van Der Gevel (The University of Queensland), and the financial of the University of Queensland.

References

Chanson, H. 2012. Momentum Considerations in Hydraulic Jumps and Bores. Journal of Irrigation and Drainage Engineering, ASCE, Vol. 138, No. 4, pp. 382-385 (DOI 10.1061/(ASCE)IR.1943-4774.0000409).

Chanson, H., Reungoat, D., Simon, B., and Lubin, P. 2011. High-Frequency Turbulence and Suspended Sediment Concentration Measurements in the Garonne River Tidal Bore. Estuarine Coastal and Shelf Science, Vol. 95, No. 2-3, pp. 298-306 (DOI 10.1016/j.ecss.2011.09.012).

Chen, J., Liu, C., Zhang, C., and Walker, H.J. 1990. Geomorphological Development and Sedimentation in Qiantang Estuary and Hangzhou Bay. Jl of Coastal Research, Vol. 6, No. 3, pp. 559-572.

Jang, J.-H., Ho, H.-Y, and Yen, C.-L. 2011. Effects of Lifting Force on Bed Topography and Bed-Surface Sediment Size in Channel Bend. Journal of Hydraulic Engineering, ASCE, Vol. 137, No. 9, pp. 911-920 (DOl: 10.1061/(ASCE)HY.1943-7900.0000402).

Khezri, N., and Chanson, H. 2012a. Undular and Breaking Tidal Bores on Fixed and Movable Gravel Beds. Journal of Hydraulic Research, IAHR, Vol. 50, No. 4, pp. 353-363 (DOI: 10.1080/00221686.2012.686200).

Khezri, N., and Chanson, H. 2012b. Inception of Bed Load Motion beneath a Bore. Geomorphology, Vol. 153-154, pp. 39-47 & 2 video movies (DOI: 10.1016/j.geomorph.2012.02.006).

Koch, C., and Chanson, H. 2008. Turbulent Mixing beneath an Undular Bore Front. Journal of Coastal Research, Vol. 24, No. 4, pp. 999-1007 (DOI: 10.2112/06-0688.1).

Liggett, J.A. 1994. Fluid Mechanics. McGraw-Hill, New York, USA.

Lighthill, J. 1978. Waves in Fluids. Cambridge University Press, Cambridge, UK, 504 pages.

Mei, R. 1992. Approximate Expression for the Shear Lift Force on a Spherical Particle at Finite Reynolds Number. Intl Jl of Multiphase Flow, Vol. 18, No. 1, pp. 145-147.

Mouazé, D., Chanson, H., and Simon, B. 2010. Field Measurements in the Tidal Bore of the Sélune River in the Bay of Mont Saint Michel (September 2010). Hydraulic Model Report No. CH81/10, School of Civil Engineering, The University of Queensland, Brisbane, Australia, 72 pages.

Reungoat, D., Chanson, H., and Caplain, B. 2012. Field Measurements in the Tidal Bore of the Garonne River at Arcins (June 2012). Hydraulic Model Report No. CH89/12, School of Civil Engineering, The University of Queensland, Brisbane, Australia, 121 pages.

Tessier, B., and Terwindt, J.H.J. 1994. "An Example of Soft-Sediment Deformations in an intertidal Environment - The Effect of a Tidal Bore. Comptes-Rendus de l'Académie des Sciences, Série II, Vol. 319, No. 2, Part 2, pp. 217-233 (in French).

Treske, A. 1994. Undular Bores (Favre-Waves) in Open Channels - Experimental Studies. Jl of Hydraulic Research,

IAHR, Vol. 32, No. 3, pp. 355-370.
Tricker, R.A.R. 1965. Bores, Breakers, Waves and Wakes. American Elsevier Publ. Co., New York, USA.